The effects of dendritic load on the firing frequency of oscillating neurons

Michael A. Schwemmer and Timothy J. Lewis*

Department of Mathematics, One Shields Ave, University of California Davis, CA 95616

Abstract

We study the effects of passive dendritic properties on the dynamics of neuronal oscillators. We find that the addition of a passive dendrite can sometimes have counter-intuitive effects on firing frequency. Specifically, the addition of a hyperpolarized passive dendritic load can either increase or decrease firing frequency. Using the theory of weak coupling, we derive an equation for the change in frequency of the neuron due to the addition of a thin passive dendrite. We show that the manner in which the addition of the passive dendrite affects firing frequency depends on the neuronal oscillator's phase response curve (PRC). The sign of the average value of the oscillator's PRC predicts whether the addition of the dendrite causes an increase or decrease in firing frequency. Furthermore, we link this phenomenon to the slope of the neuronal oscillator's frequency-applied current (*f-I*) curve.

PACS numbers: 87.19.11, 87.19.ln, 82.40.Bj

1 Introduction

Neurons can have extensive spatial geometries, but they are often modeled as single-compartment objects that ignore the spatial anatomy of the cell. This simplification is made for mathematical tractibility and computational efficiency. However, many neurons are not electrotonically compact, and single-compartment models cannot be expected to fully capture their behavior. Dendritic properties can have substantial effects on the dynamics of single neurons, as well as the activity in neuronal networks. For example, the architecture of a dendritic tree can alter the firing pattern and encoding properties of a

*Corresponding author. Tel: +530-754-9369; fax: +530-752-6635. *E-mail address*: tjlewis@ucdavis.edu

neuronal oscillator [21, 16, 18] and dendritic filtering can change the phase-locking behavior in networks of neuronal oscillators [4, 5, 20]. Even the effects of dendrites without active ionic currents are not always straight-forward. Intuitively, if the leakage reversal potential of the passive dendrite is lower than the average voltage of the oscillations, then the firing frequency of the neuronal oscillator will decrease with the addition of the dendrite (see Figure 1 (a)). Surprisingly, however, the passive hyperpolarizing dendritic "load" can sometimes increase a neuron's firing frequency (Figure 1 (b)).

In previous modeling and experimental work, Kepler et al. [15] and Sharp et al. [30] examined the influence of electrical coupling between a neuronal oscillator and a passive cell, which is analogous to a two-compartment model of a soma with a passive dendrite [20]. They demonstrated that when the oscillator has a predominantly hyperpolarized membrane potential wave-form (i.e. a short duty-cycle), the electrical load of the passive cell acted to decrease the frequency of oscillations as the strength of the electrical coupling increased. On the other hand, when the oscillator had a predominantly depolarized membrane potential wave-form (i.e. a long duty-cycle), the electrical load of the passive cell acted to initially increase the frequency of oscillations as the strength of electrical coupling increased until the frequency reached a maximum and then decreased with further increase in coupling strength. In an analogous chemical oscillator system, Dolnik et al. [6] observed similar frequency modulation when properties of the chemical load were altered rather than the waveform of the isolated oscillator.

Here, we extend the results of Kepler et al. by developing a general framework to understand the mechanisms by which dendritic load properties and intrinsic somatic properties affect the firing frequency of the neuronal oscillator. We model a neuron as an isopotential somatic oscillator attached to a thin passive dendritic cable, i.e. a "ball-and-stick" model [27]. We use the theory of weak coupling [24, 8, 17] to derive an equation for the change in the firing frequency of the neuron due to the presence of the dendrite. We then show how the frequency effects of adding a dendrite to a neuronal oscillator can be understood in terms of dendritic properties and the somatic oscillator's phase response curve. Finally, we link the effects of adding a dendrite to a neuronal oscillator to the shape of the oscillator's frequency-applied current (*f-I*) curve.

2 Ball-and-Stick Model Neuron

We model the electrical activity of a neuron using a "ball-and-stick" model [4, 5] that consists of a spherical active isopotential soma attached to a single thin passive dendrite. The dendrite is modeled as a one-dimensional passive cable of physical length L [26, 28]

$$C_m \frac{\partial v}{\partial t} = \frac{a}{2R_C} \frac{\partial^2 v}{\partial x^2} - g_{LD}(v - E_{LD}), \quad x \in (0, L), \tag{1}$$

where $v(x,t)$ is the voltage of the dendrite in mV at position x and time t, g_{LD} is the leakage conductance in the dendrite in mS/cm^2, R_C is the cytoplasmic resistance of the dendrite in $k\Omega \cdot cm$, a is the radius of the dendrite in cm, E_{LD} is the reversal potential of the leakage conductance in the dendrite in mV, and C_m is the membrane capacitance in $\mu F/cm^2$, which is assumed to be constant throughout the neuron.

Hodgkin-Huxley (HH) [12] type equations are used to model the electrical activity of the soma. An application of the conservation of current law at the junction connecting the spherical soma and the thin dendrite ($x = 0$) yields the proximal boundary condition

$$C_m \frac{\partial v}{\partial t}(0,t) = -I_{ion,S}(v(0), \vec{w}) + I + \frac{a^2}{d^2 R_C} \frac{\partial v}{\partial x}(0,t), \tag{2}$$

where $I_{ion,S}(v, \vec{w})$ represents the sum of the HH-type ionic currents (see appendix), $\vec{w}$ is a vector containing the gating variables of the ionic conductances, and d is the diameter of the soma in cm. The gating variables in the vector $\vec{w}$ are described by equations of the form $\frac{d\vec{w}}{dt} = \frac{1}{\tau_{\vec{w}}}(\vec{w}_\infty(v) - \vec{w})$. The last term in equation (2) represents the axial current flowing from the dendrite into the soma. We assume that I, which is the applied current to the soma in $\mu A/cm^2$, is chosen such that the isolated soma undergoes T-periodic (limit cycle) oscillations. We define $v_{LC}(t)$ to be the membrane potential component of the isolated somatic oscillator's limit cycle.

We assume that no current flows out the distal end of the dendrite, which yields the no flux boundary condition at the end of the dendrite ($x = L$)

$$\frac{\partial v}{\partial x}(L,t) = 0. \tag{3}$$

Note that this model is the "Rall lumped soma" model [27] with boundary conditions altered to include active conductances in the soma [5].

The Morris-Lecar model [23, 29] and a neuron model of Traub [14, 32] are used in the simulations presented here. However, similar results were obtained using several other model neurons [12, 7, 10, 1]. Furthermore, the basic analysis that we present here is general and can be applied to any neuronal oscillator.

The analysis in this paper relies on a certain combination of model parameters being sufficiently "small". To identify this small compound parameter, we nondimensionalize the model (1-3). We set $V = V(\bar{x}, \bar{t}) = \frac{v(\lambda\bar{x}, \tau_S\bar{t}) - E_L}{-E_L}$ (where E_L is the leakage reversal potential in the soma), $\bar{x} = \frac{x}{\lambda}$, $\bar{t} = \frac{t}{\tau_S}$, where $\lambda(a) = \sqrt{\frac{a}{2R_C g_{LD}}}$ is the length constant of the dendrite, and $\tau_S = \frac{C_m}{g_L}$ is the membrane time constant of the soma. The resulting nondimensional equations for the ball-and-stick model neuron are

$$g\frac{\partial V}{\partial \bar{t}} = \frac{\partial^2 V}{\partial \bar{x}^2} - (V - \bar{E}_{LD}) \tag{4}$$

$$\frac{\partial V}{\partial \bar{t}}(0, \bar{t}) = -\bar{I}_{ion,S}(V(0, \bar{t}), \vec{w}) + \bar{I} + \varepsilon(a)\frac{\partial V}{\partial \bar{x}}(0, \bar{t}) \tag{5}$$

$$\frac{\partial V}{\partial \bar{x}}\left(\frac{L}{\lambda(a)}, \bar{t}\right) = 0. \tag{6}$$

where $g = \frac{g_L}{g_{LD}}$, $\bar{E}_{LD} = \frac{E_{LD} - E_L}{-E_L}$, $\bar{I}_{ion,S}(V(0, \bar{t}), \vec{w}) = \frac{1}{-g_L E_L} I_{ion,S}((-E_L)V(0, \bar{t}) + E_L, \vec{w})$, $\bar{I} = \frac{1}{-g_L E_L} I$, and $\varepsilon(a) = \frac{a^2}{d^2 g_L R_C \lambda(a)}$. Also, $\frac{d\vec{w}}{dt} = \frac{1}{\tau_{\vec{w}}}(\vec{w}_\infty(v) - \vec{w})$ becomes $\frac{d\vec{w}}{d\bar{t}} = \frac{\tau_S}{\tau_{\vec{w}}}(\vec{w}_\infty(-E_L V(0, \bar{t}) + E_L) - \vec{w})$. We define the nondimensionalized period of the limit cycle to be $\bar{T} = \frac{T}{\tau_S}$, and the nondimensional voltage component of the isolated soma's limit cycle as $V_{LC}(\bar{t})$.

The term $\varepsilon(a)\frac{\partial V}{\partial \bar{x}}(0, \bar{t})$ in equation (5) is the nondimensional axial current at the soma-dendritic junction and is the dendrite's perturbation to the somatic membrane dynamics. To ensure that this perturbation is weak, we assume that

$$\varepsilon(a) = \frac{a^2}{d^2 g_L R_C \lambda(a)} = \frac{a^2}{d^2}\sqrt{\frac{2g_{LD}}{g_L^2 R_C a}}$$

is small. Essentially, we assume that $a \ll d$, i.e. that the radius of the dendrite is small relative to the diameter of the soma, and that $\sqrt{\frac{2g_{LD}}{g_L^2 R_C a}}$ is $O(1)$ so that $\varepsilon(a) \ll 1$.

3 Theory of Weak Coupling and Reduction to a Phase Model

The theory of weak coupling [24, 8, 17], has been widely used to analyze dynamics in networks of oscillating neurons (e.g. [9, 13, 25, 19]). The theory can also be used to analyze the dynamics of neurons under the influence of an external forcing. When this external current to an individual neuron is sufficiently weak, the complete state of the neuron can be approximated by its phase on its $\bar{T}$-periodic limit cycle, $\theta(\bar{t}) \in [0, 1)$. Furthermore, the evolution of the neuronal oscillator's phase is governed by its phase-equation

$$\frac{d\theta}{d\bar{t}} = \bar{\omega} + \Delta\bar{\omega} = \bar{\omega} + \frac{1}{\bar{T}}\int_0^{\bar{T}} Z(s)I_{ext}(s)ds, \tag{7}$$

where $\frac{d\theta}{dt}$ is the instantaneous nondimensional frequency of the neuron, $\bar{\omega} = \frac{1}{\bar{T}}$ is the nondimensional frequency of the isolated (unperturbed) somatic oscillator, and $I_{ext}(s)$ is the nondimensional $\bar{T}$-periodic external current. $Z(s)$ is the nondimensional infinitessimal phase response curve (PRC) of the neuronal oscillator. The PRC quantifies the change in phase due to a δ-function current perturbation at a particular phase on the limit cycle. The PRC can be thought of as a Green's function or impulse response function for a linear oscillator. $\Delta\bar{\omega} = \frac{1}{\bar{T}}\int_0^{\bar{T}} Z(s)I_{ext}(s)ds$ represents the modulation of the isolated oscillator's frequency due to the external current averaged over one period of the oscillations.

The theory of weak coupling can be applied to the ball-and-stick model by considering the dendritic load as the perturbation to the soma, following Crook et al. [5]. During steady oscillations in the ball-and-stick model, a $\bar{T}$-periodic current flows between the soma and dendrite, modulating the intrinsic oscillations of the soma. Therefore, we set $I_{ext}(s) = \varepsilon(a)\frac{\partial V}{\partial \bar{x}}(0,s)$, which is the (nondimensional) current at the soma-dendritic junction. As long as this modulating current is sufficiently weak, the dynamics of the ball-and-stick model can be reduced to the phase model

$$\frac{d\theta}{d\bar{t}} = \bar{\omega} + \frac{1}{\bar{T}}\int_0^{\bar{T}} Z(s)\varepsilon(a)\frac{\partial V}{\partial \bar{x}}(0,s)ds. \tag{8}$$

In order to close equation (8), $\frac{\partial V}{\partial \bar{x}}(0,\bar{t})$ needs to be determined. Using our assumption that $\varepsilon(a) \ll 1$, we can find a leading order approximation of $\frac{\partial V}{\partial \bar{x}}(0,\bar{t})$. Because the dendritic perturbation is weak, the soma clings tightly to its limit cycle so that $V(0,\bar{t}) \simeq V_{LC}(\bar{t})$. This approximation simplifies the boundary condition at the soma ($\bar{x} = 0$) and yields the leading order approximation for the system (4-6)

$$g\frac{\partial V}{\partial \bar{t}} = \frac{\partial^2 V}{\partial \bar{x}^2} - (V - \bar{E}_{LD}) \tag{9}$$

$$V(0,\bar{t}) = V_{LC}(\bar{t}) \tag{10}$$

$$\frac{\partial V}{\partial \bar{x}}\left(\frac{L}{\lambda(a)},\bar{t}\right) = 0. \tag{11}$$

System (9-11) is a first-order linear partial differential equation with $\bar{T}$-periodic forcing at one end, and the solution can be found using Fourier series. Expanding the somatic potential in a Fourier series, $V_{LC}(\bar{t}) = \frac{1}{\bar{T}}\sum_{n\in\mathbb{Z}} V_n e^{2\pi i n\bar{t}/\bar{T}}$, and solving system (9-11) yields

$$V(\bar{x},\bar{t}) = \left(\frac{V_0}{\bar{T}} - \bar{E}_{LD}\right)\frac{\cosh\left(\bar{x}-\frac{L}{\lambda(a)}\right)}{\cosh\left(\frac{L}{\lambda(a)}\right)} + \frac{1}{\bar{T}}\sum_{n\neq 0} V_n \frac{\cosh\left(b_n\left(\bar{x}-\frac{L}{\lambda(a)}\right)\right)}{\cosh\left(b_n\left(\frac{L}{\lambda(a)}\right)\right)} e^{2\pi i n\bar{t}/\bar{T}} + \bar{E}_{LD}, \quad (12)$$

where $b_n = \sqrt{1 + g2\pi i n/\bar{T}}$. Differentiating equation (12) with respect to $\bar{x}$ and evaluating at $\bar{x} = 0$ gives

$$\frac{\partial V}{\partial \bar{x}}(0,\bar{t}) = \left(\bar{E}_{LD} - \frac{V_0}{\bar{T}}\right) c_0(a) - \frac{1}{\bar{T}}\sum_{n\neq 0} c_n(a) V_n e^{2\pi i n\bar{t}/\bar{T}}, \quad (13)$$

where $c_n(a) = b_n \tanh\left(b_n \frac{L}{\lambda(a)}\right)$. Note that $c_n(a)$ are complex numbers that capture the "filtering" effects of the dendrite.

Substituting this expression for $\frac{\partial V}{\partial \bar{x}}(0,\bar{t})$back into equation (8) and expanding the PRC in a Fourier series, $Z(\bar{t}) = \frac{1}{\bar{T}}\sum_{m\in\mathbb{Z}} Z_m e^{2\pi i m\bar{t}/\bar{T}}$, yields the phase model for the ball-and-stick model

$$\begin{aligned}
\frac{d\theta}{d\bar{t}} &= \bar{\omega} + \Delta\bar{\omega} \\
&= \bar{\omega} + \varepsilon(a)\left[\frac{Z_0}{\bar{T}}\left(\bar{E}_{LD} - \frac{V_0}{\bar{T}}\right) c_0(a) - \frac{1}{\bar{T}^2}\sum_{n\neq 0} Z_{-n} V_n c_n(a)\right] \\
&= \bar{\omega} + \varepsilon(a)\left[\frac{Z_0}{\bar{T}}\left(\bar{E}_{LD} - \frac{V_0}{\bar{T}}\right) c_0(a) - \frac{2}{\bar{T}^2}\sum_{n=1}^{\infty} |Z_n V_n c_n(a)| \cos(\psi_n(a) + \gamma_n - \phi_n)\right],
\end{aligned} \quad (14)$$

where $\psi_n(a)$, γ_n, and ϕ_{-n} are the angles, in radians, corresponding to $c_n(a)$, V_n, and Z_{-n}, respectively.

Below, we will analyze the phase model in order to understand how the addition of the thin passive dendrite alters the frequency of the somatic oscillator. For convenience of physiological interpretation, the values of all quantities are reported in dimensional terms in the results section. The phase model in dimensional terms is

$$\begin{aligned}
\frac{d\theta}{dt} &= \omega + \Delta\omega \\
&= \omega + \frac{\varepsilon(a)}{\tau_S}\left[\langle z\rangle(E_{LD} - \langle v_{LC}\rangle) c_0(a) - \frac{2}{T^2}\sum_{n=1}^{\infty} |z_n v_n c_n(a)| \cos(\psi_n(a) + \gamma_n - \phi_n)\right],
\end{aligned} \quad (15)$$

where v_n and z_n are the Fourier coefficients of the membrane potential oscillations $v_{LC}(t)$ and the dimensional PRC $z(t)$, respectively, and $\langle v_{LC}\rangle = v_0/T$ and $\langle z\rangle = z_0/T$ are the mean values of $v_{LC}(t)$

and $z(t)$, respectively.

4 Results

In this section, we examine the dependence of firing frequency of the ball-and-stick neuron on the magnitude of the dendritic perturbation $\varepsilon(a)$ and the value of E_{LD}. First, we observe the behavior of the simulated model equations (1-3), and we show that this behavior is well approximated by the phase model (15). We then interpret this behavior in terms of the biophysical quantities in equation (15): $\langle z \rangle$, $\langle v_{LC} \rangle$, E_{LD}, $\varepsilon(a)$, $c_n(a)$, v_n, and z_n. Lastly, we illustrate a connection between two intrinsic properties of the isolated neuronal oscillator: the frequency-applied current curve and the average value of the PRC.

In all simulations, unless otherwise indicated, somatic dynamics are modeled by the Morris-Lecar equations with parameters given in the Appendix. We also view an increase in $\varepsilon(a)$ as an increase in the dendritic radius a. Note, however, that an increase in a also results in an increase the dendritic space constant, $\lambda(a)$.

4.1 Simulations: Passive Dendritic Load Can Either Increase or Decrease Firing Frequency

Figure 1 plots the somatic voltage traces for two different values of applied current to the soma, $I = 6.4$ $\mu A/cm^2$ (Figure 1(a)) and $I = 22.4$ $\mu A/cm^2$ (Figure 1(b)). For both cases, E_{LD} is set to -60 mV, which is hyperpolarized relative to the somatic membrane potential. Intuitively, we expect that the hyperpolarizing dendritic load should decrease the frequency of the oscillations. This is clearly the case in Figure 1(a) in which the frequency of the isolated somatic oscillator is greater than the frequency of the oscillator attached to the dendrite. However, in Figure 1(b), the frequency of the isolated somatic oscillator is lower than the frequency when the somatic oscillator is attached to the dendrite. Thus, simply by varying the current applied to the soma, the hyperpolarizing dendritic load can have a decelerating or accelerating effect on the frequency of oscillations. As mentioned earlier, this phenomenon is similar to what Kepler et al. [15] observed in a model of a neuronal oscillator electrically coupled to a passive cell.

Figure 2 shows the change in firing frequency of the full ball-and-stick model (dotted line) as a function of $\varepsilon(a)$ with $I = 6.4$ $\mu A/cm^2$ and $I = 22.4$ $\mu A/cm^2$ for two different values of E_{LD}. For a relatively hyperpolarized value of E_{LD} (-75 mV), the frequency of oscillations decreases as $\varepsilon(a)$ is increased for $I = 6.4$ $\mu A/cm^2$ (Figure 2 (a)), but the frequency increases as $\varepsilon(a)$ is increased for $I = 22.4$ $\mu A/cm^2$ (Figure 2 (a)). This agrees with the behavior seen in Figure 1. When the value of E_{LD} is

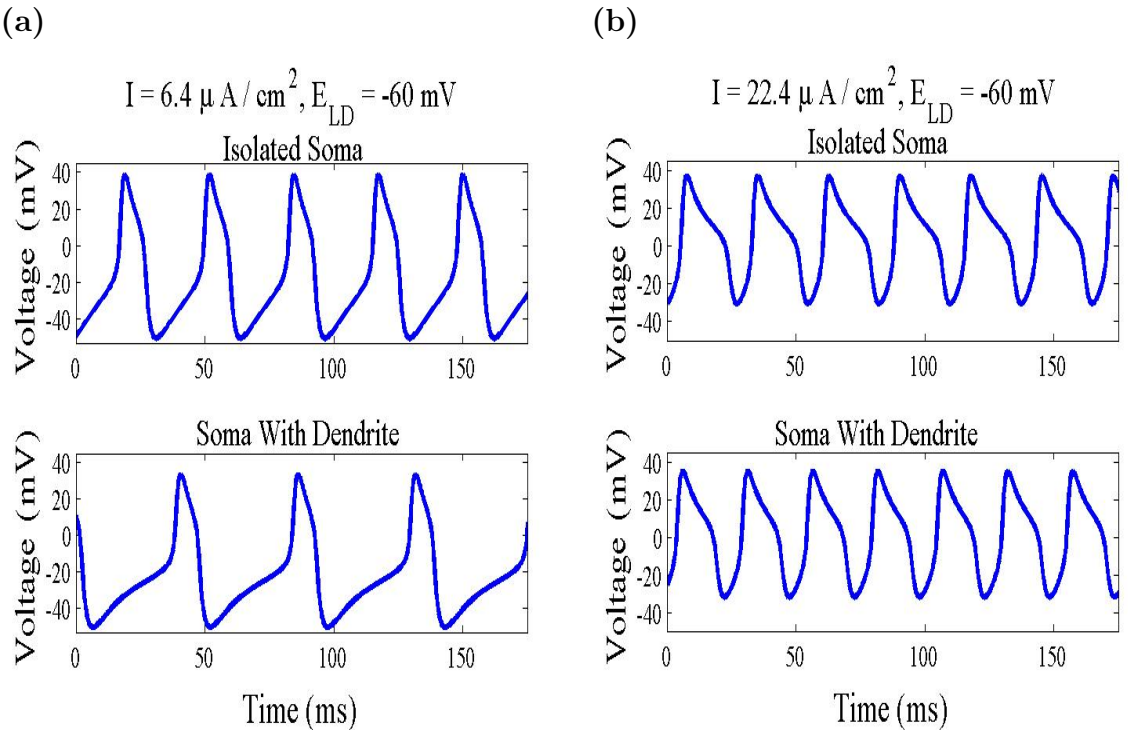

Figure 1: **The addition of a hyperpolarized dendrite can either decrease or increase firing frequency**. Voltage traces for a Morris-Lecar neuron without a dendritic cable (an isolated soma, $\varepsilon(a) = 0$) and with a passive dendritic cable ($\varepsilon(a) = 0.253$) for two different values of applied current to the soma: (a) $I = 6.4\ \mu A/cm^2$ and (b) $I = 22.4\ \mu A/cm^2$. In both cases, the dendritic leakage reversal potential E_{LD} is held at $-60\ mV$, which is hyperpolarized relative to the voltage oscillations. However, the frequency of the somatic oscillator decreases in (a) and increases in (b).

relatively depolarized (i.e. $E_{LD} = 25\ mV$, which is close to the peak of the somatic voltage), the results are reversed. That is, the frequency of oscillations increases as $\varepsilon(a)$ is increased for $I = 6.4\ \mu A/cm^2$ and decreases as $\varepsilon(a)$ is increased for $I = 22.4\ \mu A/cm^2$. Thus, the results in Figure 2(a) agree with our intuition about the effects of dendritic load: when the leakage reversal potential of the dendrite is hyperpolarized (depolarized) relative to the somatic voltage oscillations, the frequency of oscillations is decreased (increased) as the strength of the dendritic perturbation is increased. However, Figure 2(b) shows that by changing the intrinsic period of the somatic oscillator, the addition of a passive hyperpolarizing dendrite load can have a counter-intuitive effect and increase the frequency of oscillations.

4.2 Mechanisms for Frequency Changes: Insights from the Phase Model

The phase model quantitatively captures the behavior of the full model for sufficiently small values of $\varepsilon(a)$, and Figure 2 shows that it can also capture the qualitative behavior for moderate values of $\varepsilon(a)$.

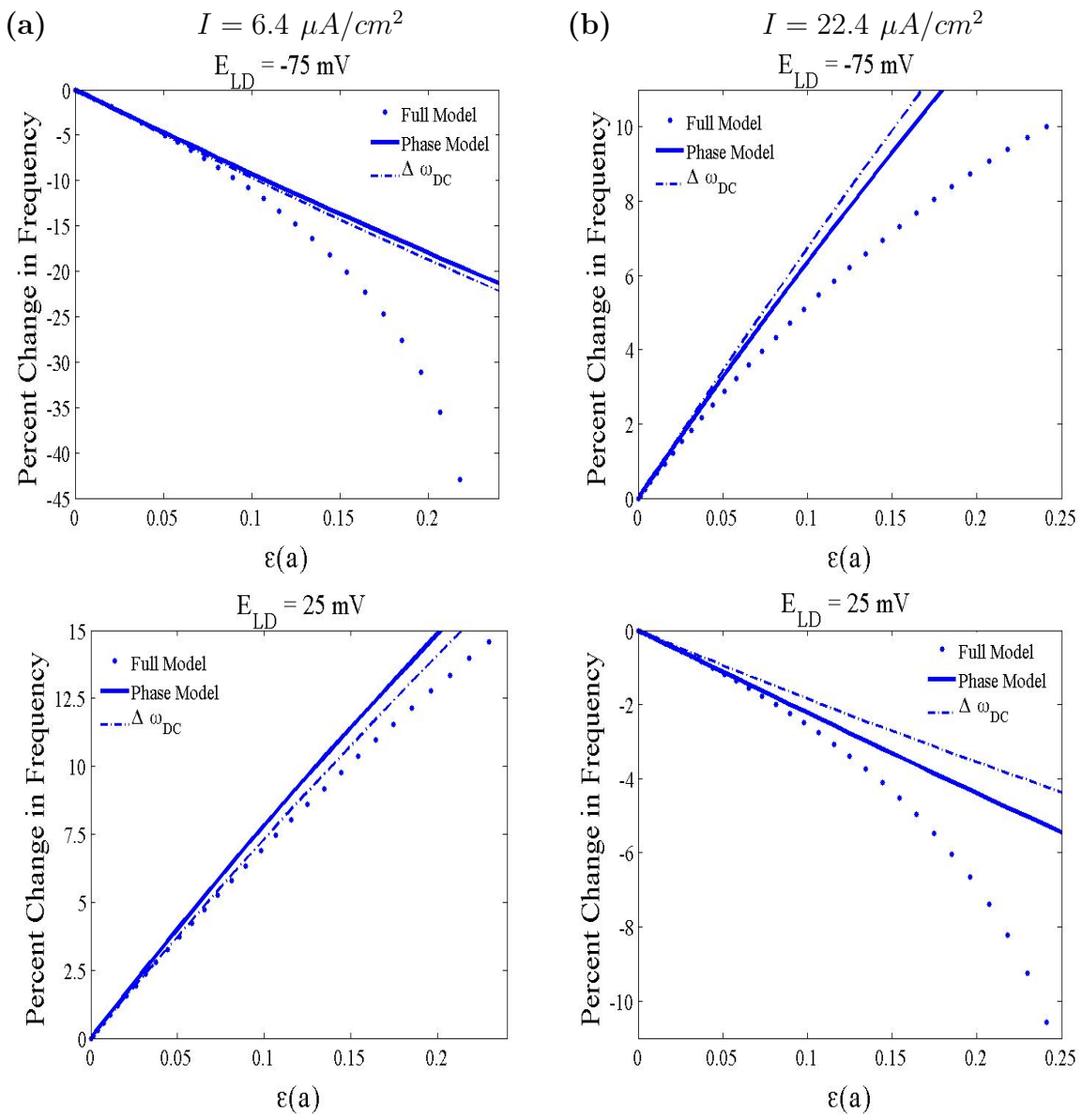

Figure 2: **Firing frequency can either increase or decrease as a function of increasing magnitude of the dendritic perturbation, $\varepsilon(a)$, depending upon the value of the dendritic leakage reversal potential and the applied current at the soma**. Percent change in firing frequency is plotted as a function of the strength of the dendritic perturbation, $\varepsilon(a)$, for hyperpolarized ($-75\ mV$) and depolarized ($25\ mV$) values of E_{LD} when (a) $I = 6.4\ \mu A/cm^2$ and (b) $I = 22.4\ \mu A/cm^2$. The dots represent results from simulations of the full ball-and-stick model, equations (1-3), the solid line represents results from simulations of the phase model, equation (15), and the dash-dotted line represents $\Delta\omega_{DC}$, equation (16). In (a), the addition of the dendrite with a hyperpolarized (depolarized) leakage reversal potential decrease (increases) the frequency of oscillations as $\varepsilon(a)$ is increased. In (b), we see the opposite effect: the addition of the dendrite with a hyperpolarized (depolarized) leakage reversal potential increases (decreases) the frequency of oscillations as $\varepsilon(a)$ is increased. Note that, for all four plots, $\Delta\omega_{DC}$ captures the tendency for the frequency to increase or decrease as a function of $\varepsilon(a)$.

Therefore, we can use the phase model to explain the effects of dendritic load on firing frequency in terms of cable properties and intrinsic properties of the neuronal oscillator. To do this, it is useful to emphasize the split in the frequency modulation term of the phase model $\Delta\omega$ into the DC ($n = 0$) component $\Delta\omega_{DC}$ and the AC ($n \neq 0$) component $\Delta\omega_{DC}$. That is, $\Delta\omega = \Delta\omega_{DC} + \Delta\omega_{AC}$, where

$$\Delta\omega_{DC} = \frac{\varepsilon(a)}{\tau_S}\langle z\rangle(E_{LD} - \langle v_{LC}\rangle)c_0(a) \tag{16}$$

$$\Delta\omega_{AC} = -\frac{\varepsilon(a)}{\tau_S}\frac{2}{T^2}\sum_{n=1}^{\infty}|z_n v_n c_n(a)|\cos(\psi_n(a) + \gamma_n - \phi_n). \tag{17}$$

Note that the DC components $\Delta\omega_{DC}$ corresponding to the examples depicted in Figure 2 accurately capture the tendency for the frequency to increase or decrease as a function of $\varepsilon(a)$. Given that the DC component plays the dominant role in determining the frequency modulation, equation (16) reveals the mechanisms underlying the phenomena described in the previous sections. Specifically, the tendency for the frequency of the oscillations to increase or decrease as a function of $\varepsilon(a)$ is determined by the sign of the product of $\langle z\rangle$ and $(E_{LD} - \langle v_{LC}\rangle)$. (Note that $c_0(a)$ is real and positive). In Figure 3, it can be seen that (a) for $I = 6.4\ \mu A/cm^2$, the average value of the PRC is positive ($\langle z\rangle = 0.0027\ mV^{-1}$) , whereas (b) for $I = 22.4\ \mu A/cm^2$, the average value of the PRC is negative ($\langle z\rangle = -0.0016\ mV^{-1}$). Therefore, when E_{LD} is less than $\langle v_{LC}\rangle$ (i.e the dendritic load is hyperpolarizing), the frequency of oscillations decreases in case (a) but increases in case (b) as $\varepsilon(a)$ increases. When E_{LD} is greater than $\langle v_{LC}\rangle$, the results are reversed. This simple explanation accounts for all of the behavior in Figure 2, and it will hold in general whenever $\Delta\omega_{DC}$ is the dominant term in $\Delta\omega$, i.e. whenever $\langle z\rangle$ is not close to zero and/or $\langle v_{LC}\rangle$ is not close to E_{LD}.

$\Delta\omega_{DC}$ (equation (16)) predicts that the effect of the dendritic load will switch between decelerating and accelerating as E_{LD} crosses $\langle v_{LC}\rangle$. Figure 4 plots the change in firing frequency as a function of E_{LD} for the full model (dotted line), the phase model (solid line), and the $\Delta\omega_{DC}$ prediction (dash line) for three different applied currents: (a) $I = 6.4\ \mu A/cm^2$ where $\langle z\rangle > 0$, (b) $I = 22.4\ \mu A/cm^2$ where $\langle z\rangle < 0$, and (c) $I = 16.6\ \mu A/cm^2$ where $\langle z\rangle$ is negative but is two orders of magnitude smaller than that in (b). As expected from the signs of $\langle z\rangle$, the dendritic load changes from having a decelerating effect to an accelerating effect in case (a) and an accelerating effect to a decelerating effect in case (b) as E_{LD} is increased. $\Delta\omega_{DC}$ predicts that the switch occurs at $\langle v_{LC}\rangle = -17.9\ mV$ for (a) and $\langle v_{LC}\rangle = 3.5\ mV$ for (b). These are close to the actual switching points, which are $E_{LD} \sim -22\ mV$ in (a) and $E_{LD} \sim 0\ mV$ in (b).

In the cases portrayed in Figure 4(a) and Figure 4(b), $\Delta\omega_{DC}$ does an excellent job of predicting

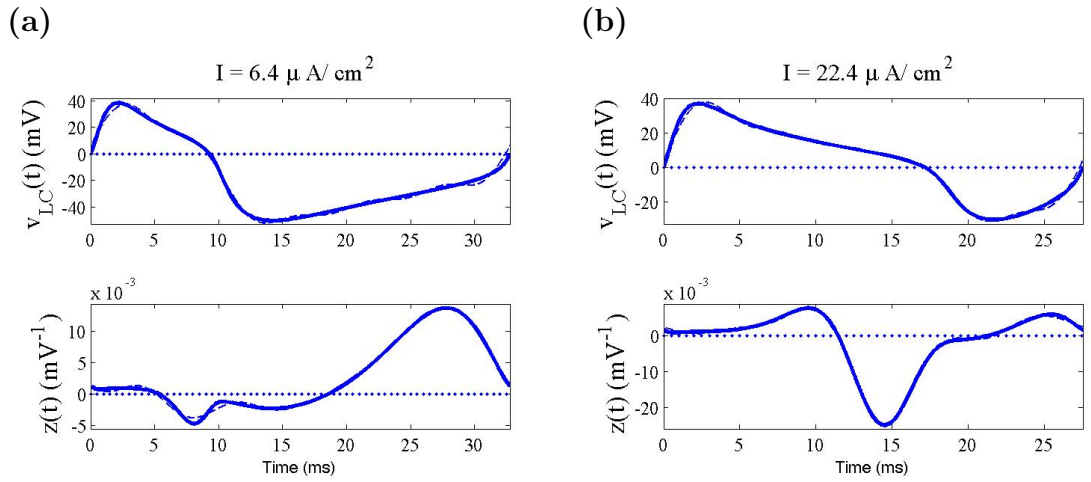

Figure 3: **Voltage component of the limit cycle for the Morris-Lecar neuron and its corresponding phase response curve.** (a) $I = 6.4\ \mu A/cm^2$ and (b) $I = 22.4\ \mu A/cm^2$. The oscillator in (a) has a positive average value of its phase response curve $\langle z \rangle = 0.0027\ mV^{-1}$ and a mean membrane potential of $\langle v_{LC} \rangle = -17.9\ mV$, while the oscillator in (b) has $\langle z \rangle = -.0016\ mV^{-1}$ and $\langle v_{LC} \rangle = 3.5\ mV$. The dashed line in all plots is the approximation to the function using the first five Fourier modes in its expansion.

both the sign and magnitude of the change in frequency over a broad range of E_{LD}. However, as E_{LD} approaches $\langle v_{LC} \rangle$, the magnitude of the DC component becomes smaller than the AC component. As a consequence, $\Delta\omega_{DC}$ incorrectly predicts the sign of frequency change in the interval between the actual and the predicted switching points. The size of this "interval of error" for the DC prediction is

$$|E_{LD} - \langle v_{LC} \rangle| = \frac{\tau_S}{\varepsilon(a)} \frac{\Delta\omega_{AC}}{\langle z \rangle\ c_0(a)} = \frac{\frac{1}{T^2} \sum_{n \neq 0} z_{-n} v_n c_n(a)}{\langle z \rangle\ c_0(a)}. \tag{18}$$

The relative magnitude of $\langle z \rangle$ as compared to the AC component in the cases in Figure 4 (a) and (b) is small and makes the interval of error small (3.5 and 3.8 mV respectively). However, for different parameters, $\langle z \rangle$ can be relatively small and $\Delta\omega_{AC}$ can be the dominant term in $\Delta\omega$. This can cause the interval of error to be large. For example, in Figure 4(c), where $\langle z \rangle = -4.31 \times 10^{-5}\ mV^{-1}$, the size of the interval of error is 132.6 mV.

Over the range of applied currents tested (4.4-23.6 $\mu A/cm^2$), $\langle z \rangle$ monotonically decreases from 0.0074 to $-0.0036\ mV^{-1}$, and the magnitude of the normalized AC components $\left|\frac{\Delta\omega_{AC}}{\varepsilon(a)}\right|$ ranges from 0.0059 to 0.027 for $a = 2 \times 10^{-6}\ cm$ ($\epsilon(a) = 0.01118$). Furthermore, $c_0(a) \sim 1$ and the magnitude of the normalized AC components $\frac{\Delta\omega_{AC}}{\varepsilon(a)}$ has a weak dependence on a for the parameters that we considered (i.e. $T \gg \tau_S$ and $L > 1.5\lambda(a)$, see appendix C). As a result, the size of the interval of error for the DC prediction

ranges from less than 1 mV near the edges of the applied current range to infinite when $\langle z \rangle = 0$ near $I = 16\ \mu A/cm^2$. The range of the applied current over which the size of the interval of error was greater than 20 mV is 14.4 to 17.6 $\mu A/cm^2$. Within this range, the frequency modulation is primarily due to the AC component and is very weak, i.e. $\Delta\omega$ is on the order of $0.01\varepsilon(a)$. The dependence of frequency modulation on E_{LD} in this range is also very weak, as is seen in Figures 4(c) and 5 and by the fact that $\Delta\omega_{AC}$ is independent of E_{LD}.

4.3 Average Value of PRC and Frequency-Applied Current (*f-I*) Curve

The above results describe the mechanisms of frequency modulation due to the dendrite in terms of the average value of the phase response curve $\langle z \rangle$, which is not a commonly considered quantity. Here, we derive the relationship between the familiar frequency-applied current (*f-I*) curve and the average value of the oscillator's phase response curve, and we then link to this relationship back to the frequency effects of the passive dendrite on neuronal oscillations.

Consider an isolated neuronal oscillator subjected to a constant applied current I, and suppose that $\omega(I)$ and $Z(s;I)$ are parameterizations of the frequency and PRC of the oscillator in terms of the applied current. Now suppose that applied current is increased by a small amount ΔI. According to the theory of weak coupling, the new frequency of the oscillator is

$$\omega(I+\Delta I) = \frac{d\theta}{dt} \simeq \omega(I) + \frac{1}{T}\int_0^T Z(s;I)\frac{\Delta I}{C_m}ds \tag{19}$$

$$= \omega(I) + \langle z(\cdot;I)\rangle \frac{\Delta I}{C_m}. \tag{20}$$

Rearranging equation (20) yields the relationship between the change in the frequency of an oscillator due to the additional applied current and average value of the oscillator's PRC

$$\frac{d\omega}{dI} \simeq \frac{1}{C_m}\frac{\omega(I+\Delta I)-\omega(I)}{\Delta I} = \frac{1}{C_m}\langle z(\cdot;I)\rangle. \tag{21}$$

Thus, the average value of an oscillator's phase response curve for a particular value of applied current normalized by the membrane capacitance is equivalent to the instantaneous slope of the oscillator's *f-I* curve at that particular applied current value. (Note that the right-hand side of equation (20) is a Taylor series of $\omega(I+\Delta I)$ with $\frac{d\omega}{dI} = \frac{\langle z(\cdot;I)\rangle}{C_m}$).

In the typical case where the DC-component $\Delta\omega_{DC}$ dominates the effect of the dendrite on firing

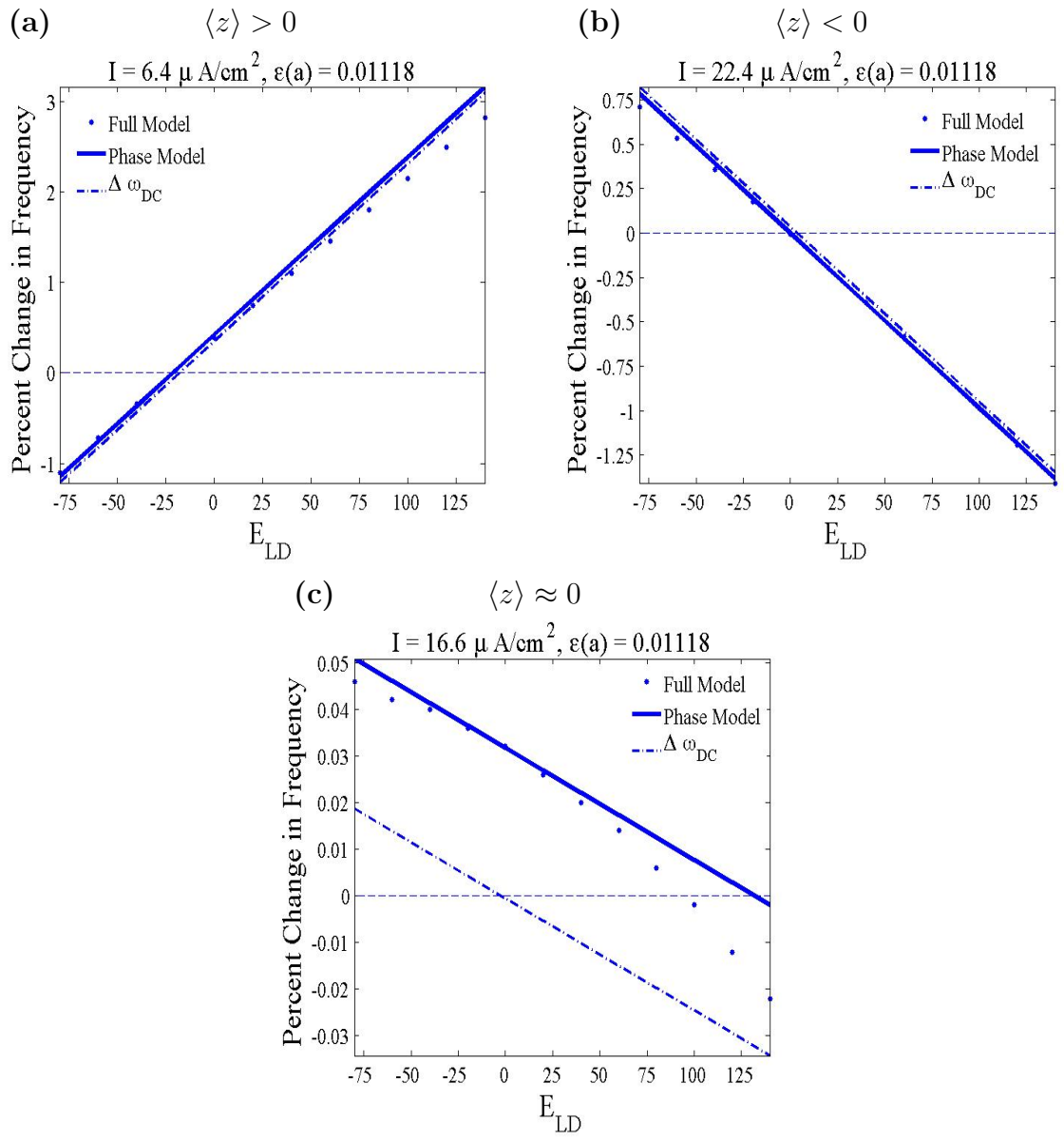

Figure 4: **Dendritic load switches its effect on frequency as the dendritic leakage reversal potential is increased**. Percent change in firing frequency is plotted as a function of the dendritic leakage reversal potential, E_{LD}, for fixed $\varepsilon(a) = 0.01118$ when (a) $\langle z \rangle > 0$, (b) $\langle z \rangle < 0$, and (c) $\langle z \rangle \approx 0$ ($I = 16.6\ \mu A/cm^2$ and $\langle z \rangle = -4.31 \times 10^{-5}\ mV^{-1}$). The dots represent simulations of full ball-and-stick model (equations (1-3)), the solid line represents simulations of the phase equation (15), and the dash-dotted line represents $\Delta\omega_{DC}$ (equation (16)). In (a), the dendritic load switches from having a decelerating effect on frequency to an accelerating effect as E_{LD} is increased. While in (b), the dendritic load switches from having an accelerating effect on frequency to a decelerating effect as E_{LD} is increased. In both cases, the 'interval of error' in which $\Delta\omega_{DC}$ incorrectly predicts the sign of frequency change is small, and $\Delta\omega_{DC}$ remains close to the full phase model prediction. When $\langle z \rangle \approx 0$ as in (c), the interval of error is considerably larger. However, the frequency modulation effects are much smaller in (c) than in either (a) or (b).

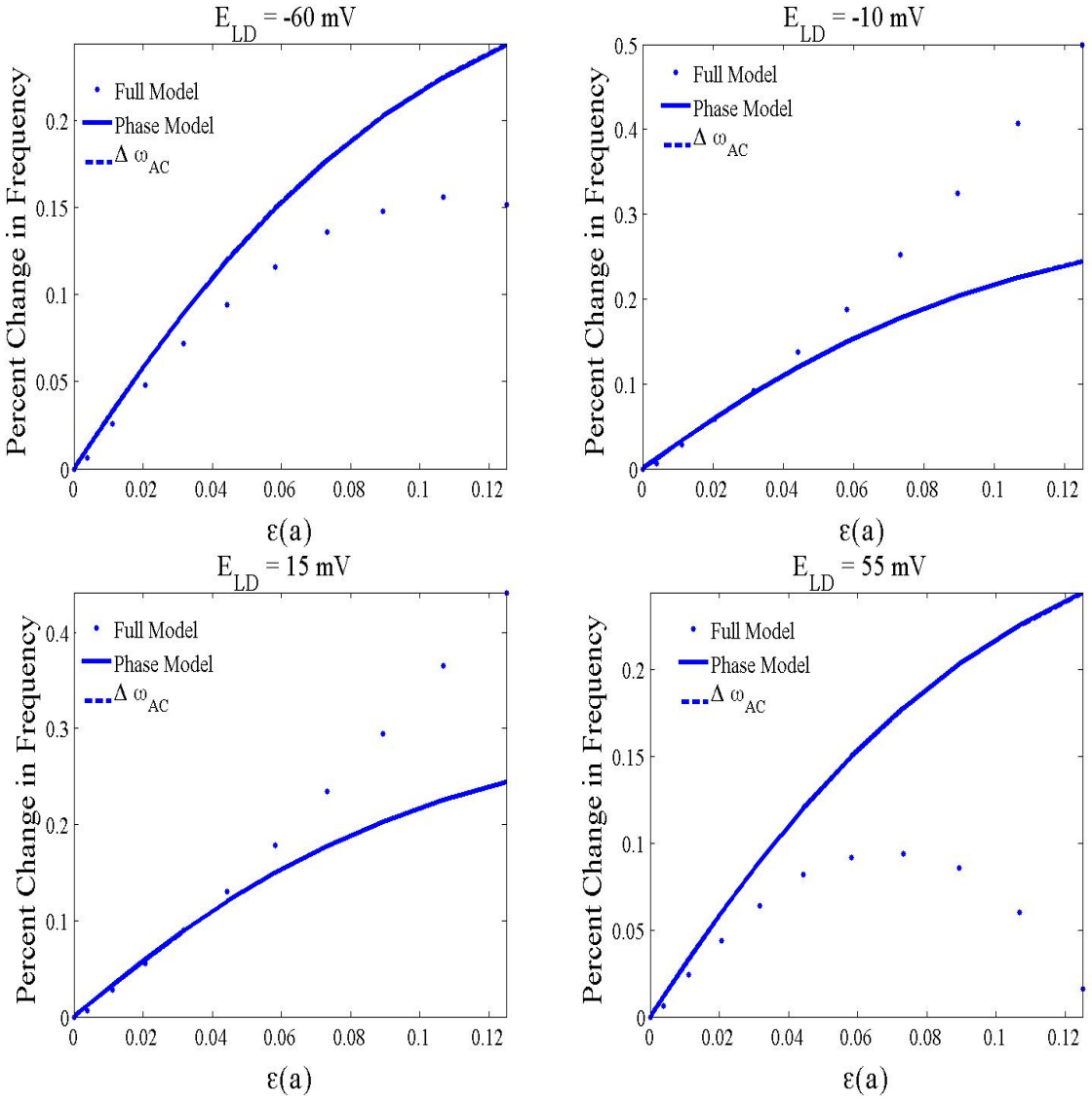

Figure 5: **When the average value fo the PRC $\langle z \rangle \approx 0$, $\Delta\omega_{AC}$ dominates the behavior of the phase model**. Percent change in firing frequency is plotted as a function of $\varepsilon(a)$ when $\langle z \rangle \approx 0$ ($I = 16.32$ $\mu A/cm^2$ and $\langle z \rangle = 1.39 \times 10^{-7}$ mV^{-1}).The dots represent simulations of full ball-and-stick model (equations (1-3)). The simulations of the phase equation (15) (solid line) and $\Delta\omega_{AC}$ (equations (16)) (the dashed line) overlap for the four values of the dendritic leakage reversal potential E_{LD}, indictating that $\Delta\omega \simeq \Delta\omega_{AC}$ in this case. This is due to the fact that $\Delta\omega_{DC}$ is close to zero as $\langle z \rangle \approx 0$. Also, because $\Delta\omega_{AC}$ is independent of E_{LD}, the phase model behavior remains virtually unchanged for the four different values of E_{LD}. Note that the frequency modulation effects of the dendrite are smaller than those seen in Figure 2.

frequency, we can subsitute $C_m \frac{d\omega}{dI}$ for $\langle z(\cdot; I) \rangle$ into equation (16) to obtain

$$\frac{d\theta}{dt} \simeq \omega + \frac{\varepsilon(a)}{\tau_S} C_m \frac{d\omega}{dI}(E_{LD} - \langle v_{LC} \rangle) c_0(a) \tag{22}$$

$$\simeq \omega + \frac{d\omega}{dI} \varepsilon(a) g_L (E_{LD} - \langle v_{LC} \rangle) c_0(a). \tag{23}$$

That is, the change in frequency of a neuronal oscillator due to the addition of a passive dendrite is simply given by the product of the average axial current flowing between the dendrite and the soma (i.e. a *constant* current) and the instantaneous slope of the neuronal oscillator's *f-I* curve.

Figure 6(a) illustrates the relationship between the *f-I* curve, it's derivative and the average of the PRC $\langle z \rangle$ for the isolated Morris-Lecar neuron (i.e. the soma) as a function of applied current. For this model neuron, the *f-I* curve is non-monotonic: the frequency initially increases with increasing current, but the frequency reaches a maximum and then decreases with increasing current. As a result, the addition of a strictly hyperpolarizing dendritic load will lead to an decrease in firing frequency for relatively low applied currents, but there will be a "counter-intuitive" increase in firing frequency for relatively high applied currents, as shown in Figure 6(b).

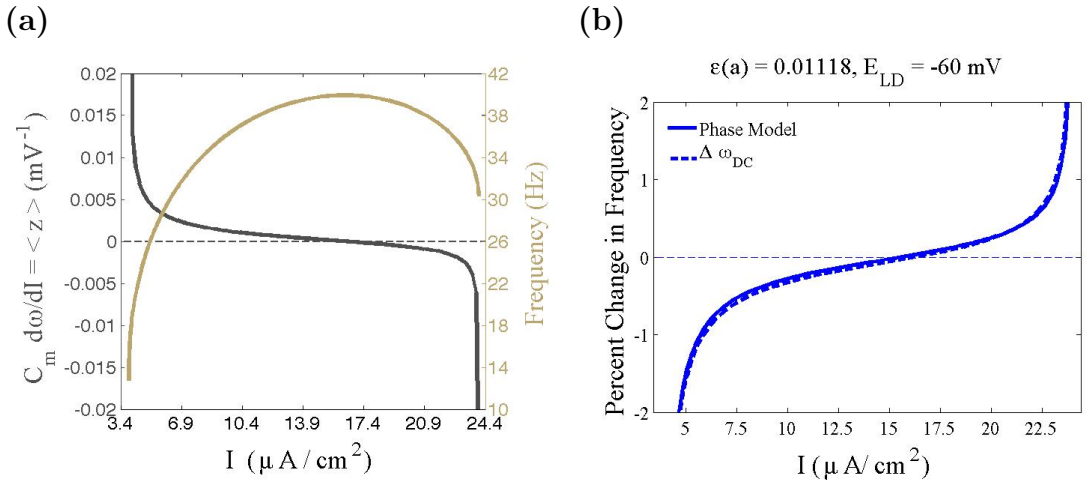

Figure 6: **(a) Frequency and average value of the somatic oscillator's phase response curve $\langle z \rangle$ versus I, for an isolated Morris-Lecar neuron**. The plot of $\frac{d\omega}{dI}$ is identical to that of $\langle z \rangle$. The point at which the frequency of the limit cycle oscillations (gold curve) reaches a maximum occurs at the same point that $\langle z \rangle$ (black curve) reaches zero and subsequently becomes negative as I is increased. **(b) Change in frequency due to the presence of the dendrite, $\Delta\omega$, as a function of I.** The solid line plots $\Delta\omega$ and the dashed line plots $\Delta\omega_{DC}$. In this case, the dendrite is hyperpolarized relative to the voltage oscillations, i.e. $\Delta I < 0$. Thus, the dendritic load has a decelerating effect on frequency when $\langle z \rangle > 0$ and an accelerating effect when $\langle z \rangle > 0$. Note that for these values of E_{LD} and $\varepsilon(a)$, $\Delta\omega_{DC}$ remains very close to $\Delta\omega$, and both $\Delta\omega$ and $\Delta\omega_{DC}$ retain the shape of the $\langle z \rangle$ versus I curve.

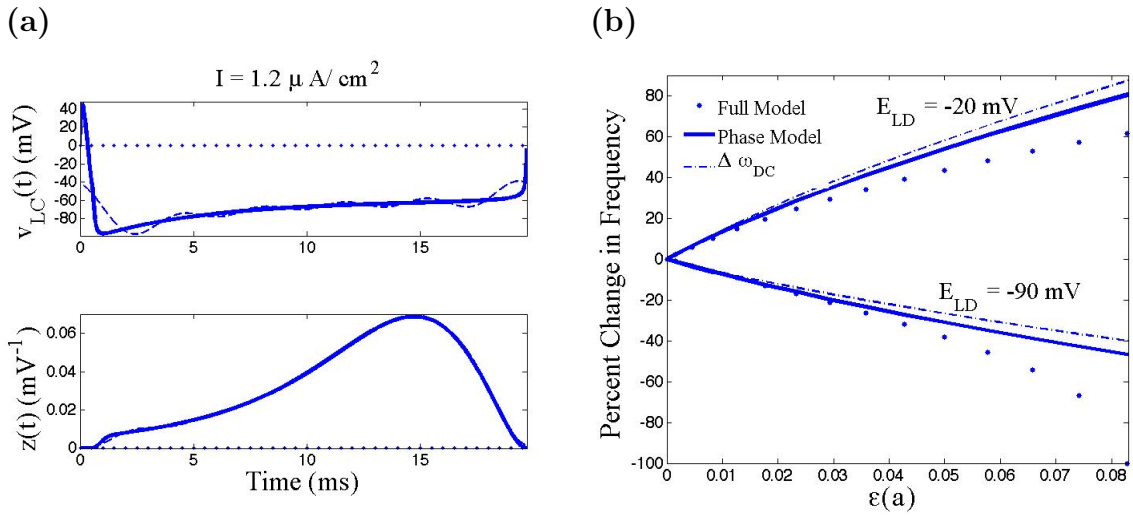

Figure 7: $\Delta\omega_{DC}$ **dominates the behavior of the phase model for a more detailed model neuronal oscillator.** (a) Voltage component of the limit cycle for the Traub et al. model neuron [32] and its corresponding phase response curve. The dotted line in both plots is the approximation to the function using the first five Fourier modes. $\langle v_{LC}\rangle = -68.02\ mV$ and $\langle z\rangle = 0.032\ mV^{-1}$. (b) Percent change in firing frequency is plotted as a function of the strength of the dendritic perturbation, $\varepsilon(a)$, for a hyperpolarized ($-90\ mV$) and depolarized ($-20\ mV$) value of E_{LD} when $I = 1.2\ \mu A/cm^2$. The dots represent results from simulations of the full ball-and-stick model (equations (1-3)) the solid line represents results from simulations of the phase model (equation (15)) and the dash-dotted line represents $\Delta\omega_{DC}$ (equation (16)). As in Figure 2(a), the addition of the dendrite with a hyperpolarized leakage reversal potential decreases the frequency of oscillations as $\varepsilon(a)$ is increased while the addition of the dendrite with a depolarized leakage reversal potential increases the frequency of oscillations as $\varepsilon(a)$ is increased. It is important to note that $\Delta\omega_{DC}$ remains close to the phase model for both values of the dendritic leakage reversal potential.

5 Discussion

In this article, we examine how a passive dendritic load affects the firing frequency of a ball-and-stick model neuron. Using the theory of weak coupling, we derive an analytical expression that relates the change in frequency to the phase response properties of the model neuron and the properties of the dendrite [5]. We then elucidate the mechanisms underlying the counter-intuitive increases in firing frequency that can occur due to a hyperpolaring dendritic load. Appendix D applies similar analysis to the an oscillator electrically coupled to a passive compartment in which case very similar results are obtained.

Three main observations in this article allow the clear identification of the fundamental mechanisms underlying the changes in a neuron's firing frequency due to the addition of a dendritic load: (1) The DC-component of the analytical expression for firing frequency, $\Delta\omega_{DC}$, typically dominates higher modes. This is the case unless the average of the PRC $\langle z\rangle$ is tuned to be close to zero and/or the average of the oscillating membrane potential $\langle v_{LC}\rangle$ is tuned to be close to the reversal potential of the dendrite

E_{LD}. (2) The form of $\Delta\omega_{DC}$ indicates that the change in frequency due to the dendritic load is primarily determined by the product $\langle z\rangle(E_{LD} - \langle v_{LC}\rangle)$. Along with the observation 1, this implies that the effect of a passive dendritic load on a neuron's firing frequency is equivalent to that of an additional constant current. (3) The average value of a PRC $\langle z\rangle$ is equal to the instantaneous slope of the neuron's *f-I* curve. Thus, when $\langle z\rangle > 0$ or equivalently $\frac{df}{dI} > 0$, the addition of a hyperpolarizing dendritic load causes the neuron's frequency to decrease. On the other hand, when $\langle z\rangle < 0$ or equilavently $\frac{df}{dI} < 0$, the addition of a hyperpolarizing dendritic load leads to a "counter-intuitive" decrease in the firing frequency of a neuron. Note that the failure of our intuition for this behavior arises from the preconception that frequency always increases with increased applied current.

The mechanisms discussed above provide a general framework for understanding the influence of passive dendritic properties on the firing frequency of neuronal oscillators. The numerical results presented section 4 are for the Morris-Lecar model, but we have obtained similar results for several other neuronal models. For example, Figure 7 shows that the DC component quantitatively captures the frequency modulation when somatic dynamics are described by the Traub et al. [14, 32] model, which is a more biophysically detailed model (see appendix for equations). In fact, $\langle z\rangle$ is relatively large over the entire oscillatory range for the Traub et al. model, and therefore the DC component correctly predicts the frequency modulation. On the other hand, $\langle z\rangle$ is always positive, and therefore the counter-intuitive increase in response to the addition of a hyperpolarizing dendritic load will not occur. Similar behavior would occur for any stereotypical "type-I" neuron [9].

Skinner et al. [31] found that cultured stomatogastric ganglion (STG) neurons can exhibit either monotonic or non-monotomic *f-I* curves and that neurons are able to switch between these two response properties with pharmacological manipulation. They also demonstrated that modest changes of parameters can switch model neurons between these two behaviors. Furthermore, they showed that, when model neurons with non-monotonic *f-I* curves are coupled by reciprocal inhibition, the frequency of the network can increase beyond the maximum frequency for a isolate cell. The mechanisms responsible for this phemonena is intimately related to those described in this article

As mentioned before, the well-known modeling study by Kepler et al. [15] has previously examined the effects of electrically coupling a neuronal oscillator to a hyperpolarized passive cell in context of central pattern generators in the lobster stomatogastric ganglion. Kepler et al. found that, if the membrane potential of the neuronal oscillator has a short duty-cycle (i.e. a predominantly hyperpolarized wave-form as in Figure 3(a)), the electrical load of the passive cell acts to decrease the frequency of oscillations as the strength of the electrical coupling is increased. On the other hand, if the membrane potential of the neuron has a long duty-cycle (i.e. a predominantly depolarized wave-form as in Figure 3(b)), the

electrical load of the passive cell can increase the frequency of oscillations. Their explanation for this phenomenon was based on the balance of inward and outward currents in the oscillator compartment. More specifically, they postulated that, during the depolarized phase of the neuronal oscillations, the hyperpolarized passive compartment acts to more rapidly repolarize the neuronal oscillator and therefore acts to decrease period of oscillation. On the other hand, during the subthreshold phase of the neuronal oscillations, the hyperpolarized passive compartment acts to slow the rate of depolarization towards threshold, and therefore it acts to increase period of oscillation. When the neuronal oscillators has a short duty-cycle, the cycle is dominated by the subthreshold phase and therefore the net effect of the passive load is to decrease the frequency of oscillations. When the neuronal oscillators has long duty-cycle, the cycle is dominated by the depolarized phase and therefore the net effect of the passive load is to increase the frequency of oscillations.

Inherent in the explanation provided by Kepler et al. are the assumptions that the phase response curve of the oscillator will always be negative during the depolarized phase of the cycle and positive during the subthreshold phase of the cycle. Although this is the case for the simple model neuron that they used in their study, phase response properties of neuronal oscillators are typical more complicated than this (see Figure 3). For instance, neurons often have phase response curves with negative portions during the subthreshold phase [22]. The explanation provided in this article in terms of the oscillator's phase response curve is still conceptually simple and yet is more general in the sense that it can be applied to any oscillator.

The analysis presented in this paper relies on the assumptions that (1) the dendrites are thin relative to the diameter of the soma, and therefore only weakly perturb the somatic dynamics, and (2) the dendrites are passive and do not contain active membrane conductances. If the dendritic perturbation to a somatic oscillator is large and/or there are highly active conductances in the dendrites, the dendritic load can fundamentally change firing dynamics, e.g. quenching oscillations altogether or inducing bursting dynamics [2, 21], in which case our analysis breaks down. On the other hand, simulations show that the theory qualititatively predicts the firing effects of moderately sized dendritic perturbations despite the fact that the analysis takes the weak perturbation limit. Furthermore, our analysis can readily be extended to include weakly nonlinear conductances in the dendrites [11, 3]. We note however that we have found no fundamental changes in the results for this case. These observations suggest that the mechanisms underlying frequency modulation described here are applicable to a range of biologically relevant situations.

A Morris-Lecar Neuron

$$C_m \frac{dv}{dt} = -g_{Ca} m_\infty(v(t))(v(t) - E_{Ca}) - g_K w(v(t) - E_K) - g_L(v(t) - E_L) + I$$
$$\frac{dw}{dt} = \phi \frac{w_\infty(v(t)) - w}{\tau_w(v(t))}$$

where

$$m_\infty(v) = \frac{1}{2}\left[1 + \tanh\left(\frac{v - V_1}{V_2}\right)\right]$$
$$w_\infty(v) = \frac{1}{2}\left[1 + \tanh\left(\frac{v - V_3}{V_4}\right)\right]$$
$$\tau_w(v) = \frac{1}{\cosh\left(\frac{v - V_3}{2V_4}\right)}$$

and

$C_m = 1\ \mu F/cm^2$	$g_{Ca} = 0.6\ mS/cm^2$	$g_K = 0.8\ mS/cm^2$
$g_L = 0.2\ mS/cm^2$	$E_{Ca} = 100\ mV$	$E_K = -80\ mV$
$E_L = -50\ mV$	$V_1 = 0\ mV$	$V_2 = 15\ mV$
$V_3 = 0\ mV$	$V_4 = 15\ mV$	$\phi = 0.08\ ms^{-1}$

The cable parameters with the Morris-Lecar neuron are

$g_{LD} = 0.5\ mS/cm^2$	$d = .002\ cm$	$R_C = 0.1\ k\Omega \cdot cm$
$L = .02\ cm$		

B Traub model soma

$$C_m \frac{dv}{dt} = -g_{Na} m^3 h(v(t) - E_{Na}) - g_K n^4 (v(t) - E_K) - g_L(v(t) - E_L) + I$$
$$\frac{dm}{dt} = \alpha_m(v)(1 - m) - \beta_m(v)m$$
$$\frac{dh}{dt} = \alpha_h(v)(1 - h) - \beta_h(v)h$$
$$\frac{dn}{dt} = \alpha_n(v)(1 - n) - \beta_n(v)n$$

where

$$\alpha_m(v) = 1.28\frac{(v+54)/4}{1-\exp(-(v+54)/4)} \qquad \beta_m(v) = 1.4\frac{(v+27)/5}{\exp(-(v+27)/5)-1}$$
$$\alpha_h(v) = 0.128\exp(-(v+50)/18) \qquad \beta_h(v) = 4.0\frac{1}{1+\exp(-(v+27)/5)}$$
$$\alpha_n(v) = 0.16\frac{(v+52)/5}{1-\exp(-(v+52)/5)} \qquad \beta_n(v) = 0.5\exp(-(v+57)/40)$$

and

$$C_m = 1\ \mu F/cm^2 \qquad g_{Na} = 100\ mS/cm^2 \qquad g_K = 80\ mS/cm^2$$
$$g_L = 0.2\ mS/cm^2 \qquad g_{LD} = 0.5\ mS/cm^2 \qquad E_{Na} = 50\ mV$$
$$E_K = -100\ mV \qquad E_L = -67\ mV$$

The cable parameters with the Traub model soma are

$$g_{LD} = 0.5\ mS/cm^2 \qquad d = .002\ cm \qquad R_C = 0.1\ k\Omega \cdot cm$$
$$L = .01\ cm$$

C Dendritic Effects in the Ball-and-Stick Phase Model

Recall that the "filtering" effects of the dendrite are captured by $c_n(a)$ in equation (15). In this section, we show that the $c_n(a)$ terms increase more slowly than the Fourier components v_n and z_n decay and that, for the parameters considered here, $|c_n(a)| \approx 1$ for small n. Therefore, the higher order cable properties of the dendrite (i.e. effects beyond the leakage reversal potential, E_{LD}) do not greatly influence the behavior of the phase model for small n. Moreover, it is most often the case that the Fourier series of the phase response curve is dominated by the first few modes (see Figures 3 and 7). Therefore, even if $\varepsilon(a)\frac{\partial V}{\partial x}(0,t)$ contains higher modes in its Fourier expansion, they will be 'zeroed out' when multiplied by the PRC. Thus, the phase model will not be greatly influenced by the cable properties and will be dominated by the first few modes of the Fourier expansion of the $\Delta\omega$ term.

Recall that $c_n(a) = b_n \tanh(b_n \frac{L}{\lambda(a)})$, with $b_n = \sqrt{1 + \frac{g_L}{g_{LD}} 2\pi i n/\bar{T}}$. For a sufficiently long dendrite $\frac{L}{\lambda(a)} \geq 1.5$, $|\tanh(b_n \frac{L}{\lambda(a)})| \in [0.9, 1.3]$. Thus, $c_n(a) \approx b_n$. Using the fact that the nondimensional period, $\bar{T}$, is equal to the dimensional period, T, divided by the somatic membrane time constant, τ_S, and the fact that $\tau_D = \frac{C_m}{g_{LD}}$, we can rewrite $c_n(a)$ as

$$c_n(a) \approx b_n = \sqrt{1 + \frac{\tau_D}{\tau_S} 2\pi i n \frac{\tau_S}{T}} = \sqrt{1 + \frac{\tau_D}{T} 2\pi i n}. \tag{24}$$

The magnitude and angle of the $c_n(a)$ terms is then given by

$$|c_n(a)| = \left(1 + n^2 \left(\frac{\tau_D}{T} 2\pi\right)^2\right)^{\frac{1}{4}} \tag{25}$$

$$\phi_n = \frac{1}{2} \arctan(2\pi n \frac{\tau_D}{T}). \tag{26}$$

Thus, $|c_n(a)|$ increases like $n^{\frac{1}{2}}$. This implies that the effect of dendrite acts to amplify the higher modes in the Fourier series. However, if $\frac{\tau_D}{T} \ll 1$, then $|c_n(a)| \approx 1$ for small n.

For our simulations, the dendritic membrane time constant, τ_D, is set at 2 ms, and the space constant, $\lambda(a)$, ranges from $O(10^{-3})$ to $O(10^{-2})$ cm for the values of dendritic radii that were used. For the Morris-Lecar and Traub et al. model neurons, $\frac{\tau_D}{T} \sim O(10^{-1})$. Thus, due to the facts that the Fourier coefficients z_n rapidly decay and that $|c_n(a)| \approx 1$ for small n, the higher order cable properties have a minimal effect on the phase model.

D Two-Compartment Model

In this section we present the phase model reduction for the two compartment model of a soma electrically coupled to a dendritic compartment. In this case, the phase model can be obtained using two different limits: the limit of weak electrical coupling and the limit of a large oscillator compartment attached to a smaller dendritic compartment. However, in both limits, the behavior of the phase model qualitatively matches that of the phase model derived from the ball-and-stick model. Thus, our explanation for the non-intuitive frequency effects seen in the cable model can be directly applied to the two-compartment model studied in Kepler et al. [15].

The soma is modeled as an isopotential compartment with Hodgkin-Huxley currents and the dendrite is modeled as a passive compartment electrically coupled to the soma [20]

$$C_m \frac{dv_S}{dt} = -I_{ion,S}(v_S(t), \vec{w}) + I + g_C \left(\frac{a_D}{a_S}\right)^2 (v_D - v_S) \tag{27}$$

$$C_m \frac{dv_D}{dt} = -g_{LD}(v_D - E_{LD}) + g_C(v_S - v_D), \tag{28}$$

where $v_S(t)$ and $v_D(t)$ represent the voltage, in mV, of the somatic and dendritic compartment, respectively, at time t, g_C is the gap junctional conductance in mS/cm^2, a_S and a_D represent the radii of the somatic and dendritic compartments, respectively, in cm, and $I_{ion,S}(v, \vec{w})$, $\bar{I}$, g_{LD}, C_m, and E_{LD} are the same as in the ball-and-stick model. In addition, I is assumed to be large enough so that the soma

undergoes periodic firing, i.e. limit cycle oscillations.

Let $V_{S,D} = V_{S,D}(t) = \frac{v_{S,D}(\tau_D \bar{t}) - E_L}{-E_L}$ (where E_L is the leakage reversal potential in the soma), $\bar{t} = \frac{t}{\tau_D}$, and $\tau_D = C_m/g_{LD}$ is the membrane time constant of the dendritic compartment. Then, our equations become

$$\frac{dV_S}{d\bar{t}} = -\bar{I}_{ion,S}(V(\bar{t}), \vec{w}) + \bar{I} + \varepsilon\gamma(V_D - V_S) \tag{29}$$

$$\frac{dV_D}{d\bar{t}} = -(V_D - \bar{E}_{LD}) + \varepsilon(V_S - V_D), \tag{30}$$

where $\gamma = \left(\frac{a_D}{a_S}\right)^2$, $\varepsilon = \frac{g_C}{g_{LD}}$, and $\bar{E}_{LD}$, $\bar{I}_{ion,S}(V(\bar{t}), \vec{w})$, and I are the same as for the ball-and-stick model.

There are two possible approaches to the phase reduction at this point: (1) assume that ε is the small parameter, or (2) assume that γ is the small parameter. Let us first examine the case where ε is small and γ is $O(1)$.

As with the ball-and-stick model, we can reduce the dynamics of our two compartment model to a single phase equation by assuming that $g_C \ll g_{LD}$ and that γ is $O(1)$. Note, in this case, our assumption is that the coupling between the two compartments is what we are assuming is small while the ratio of the radii is assumed to be $O(1)$. Since ε appears in both equations (29) and (30), both compartments will be behaving very similarly to their unperturbed ($\varepsilon = 0$) counterparts. Thus, the dendritic compartment will go to its steady state, $\bar{E}_{LD}$, and the membrane potential of the somatic compartment will go to its limit cycle, $V_{LC}(\bar{t})$. Our phase equation is then

$$\frac{d\theta}{d\bar{t}} = \bar{\omega} + \Delta\bar{\omega} = \bar{\omega} + \frac{\varepsilon\gamma}{\bar{T}} \int_0^{\bar{T}} Z(s)(\bar{E}_{LD} - V_{LC}(s))ds, \tag{31}$$

where $\varepsilon\gamma(\bar{E}_{LD} - V_{LC})$ is the nondimensional coupling current under the assumption that both V_S and V_D cling tightly to their steady states. Expanding $Z(\bar{t})$ and $V_{LC}(\bar{t})$ in Fourier series yields

$$\frac{d\theta}{d\bar{t}} = \bar{\omega} + \varepsilon\gamma\langle Z\rangle(\bar{E}_{LD} - \langle V_{LC}\rangle) - \frac{\varepsilon\gamma}{\bar{T}^2} \sum_{n\neq 0} Z_{-n}V_n. \tag{32}$$

where V_n are the coefficients of V_{LC}, Z_n are the coefficients of Z, and we have replaced $V_0/\bar{T}$ and $Z_0/\bar{T}$ with $\langle V_{LC}\rangle$, and $\langle Z\rangle$ as in equation (15). Note that this is the same as the phase equation for the ball-and-stick model without the terms describing the influence of the cable, i.e. $c_n(a)$.

Next, let us assume that γ is small and that ε is $O(1)$. In this case, we are assuming that the somatic

compartment is much larger than the dendritic compartment. Thus, the dendrite will have a minimal effect on the dynamics of the soma, implying that the membrane potential of the somatic compartment will cling to its limit cycle, $V_{LC}(\bar{t})$, while the somatic compartment will have an $O(1)$ effect on the dynamics of the dendritic compartment. Our phase equation is then

$$\frac{d\theta}{d\bar{t}} = \bar{\omega} + \Delta\bar{\omega} = \bar{\omega} + \frac{\varepsilon\gamma}{\bar{T}} \int_0^{\bar{T}} Z(s)(V_D(s) - V_{LC}(s))ds, \tag{33}$$

where the first order approximation to $V_D(\bar{t})$ is found by solving

$$\frac{dV_D}{d\bar{t}} = -(V_D - \bar{E}_{LD}) + \varepsilon(V_{LC}(\bar{t}) - V_D). \tag{34}$$

Solving the above equation using Fourier series and plugging the result into equation (33) yields

$$\frac{d\theta}{d\bar{t}} = \bar{\omega} + \gamma\langle Z\rangle(\bar{E}_{LD} - \langle V_{LC}\rangle)\left[\frac{\varepsilon}{1+\varepsilon}\right] - \frac{\gamma}{\bar{T}^2}\sum_{n\neq 0} Z_{-n}V_n c_n, \tag{35}$$

where $c_n = \frac{\varepsilon(1+2\pi in/\bar{T})}{2\pi in/\bar{T}+(1+\varepsilon)}$. Thus, in this limit, there are filtering effects due to the addition of the dendritic compartment. Recall that time was nondimensionalized using τ_D. This implies that $\bar{T} = T/\tau_D$, where T is the dimensional period of oscillations. Therefore, the magnitude of the c_n terms can be written as

$$|c_n| = \varepsilon\left(\frac{1 + (2\pi n\frac{\tau_D}{T})^2}{(2\pi n\frac{\tau_D}{T})^2 + (1+\varepsilon)^2}\right)^{\frac{1}{2}}. \tag{36}$$

Equation (36) limits to 1 as $n \to \infty$. When $\frac{\tau_D}{T} \ll 1$, $|c_n| \approx \frac{\varepsilon}{1+\varepsilon}$ for small n, which implies that the filtering effects are minimal.

In both scenarios presented above, the phase models qualitatively match the dynamics of the phase model derived from the ball-and-stick model.

References

[1] L.F. Abbott. Lapicques introduction of the integrate-and-fire model neuron (1907). *Brain Res. Bull.*, 50(5-6):303–304, 1999.

[2] A. Bose and Booth V. Bursting in 2-compartment neurons: A case study of the Pinsky-Rinzel model. In S. Coombes and P. Bressloff, editors, *Bursting: The genesis of rhythm in the nervous system*, pages 123–144. World Scientific, 2005.

[3] P.C. Bressloff. Resonantlike synchronization and bursting in a model of pulse-coupled neurons with active dendrites. *J. Comput. Neurosci.*, 6:237–249, 1999.

[4] P.C. Bressloff and S. Coombes. Synchrony in an array of integrate-and-fire neurons with dendritic structure. *Physical Review Letters*, 78:4665–4668, 1997.

[5] S.M. Crook, G.B. Ermentrout, and J.M. Bower. Dendritic and synaptic effects in systems of coupled cortical oscillators. *J. Comp. Neurosci.*, 5:315–329, 1998.

[6] M. Dolnik, T.S. Gardner, I. R. Epstein, and J. J. Collins. Frequency control of an oscillatory reaction by reversible binding of an autocatalyst. *Phys. Rev. Lett.*, 82(7):1582–1585, 1999.

[7] A. Erisir, D. Lau, B. Rudy, and C.S. Leonard. Function of specific k+ channels in sustained high-frequency firing of fast-spiking neocortical interneurons. *J. Neurophysiol.*, 82:2476–2489, 1999.

[8] G.B. Ermentrout. n:m phase-locking of weakly coupled oscillators. *J. Math. Bio.*, 12:327–342, 1981.

[9] G.B. Ermentrout. Type 1 membranes, phase resetting curves, and synchrony. *Neural Computation*, 8:1979–1001, 1996.

[10] R. FitzHugh. Impulses and physiological states in models of nerve membrane. *Biophys. J.*, 1(6):445–466, 1961.

[11] J. A. Goldberg, C. A. Deister, and C. J. Wilson. Response Properties and Synchronization of Rhythmically Firing Dendritic Neurons. *J. Neurophysiol.*, 97(1):208–219, 2007.

[12] A. Hodgkin and A. Huxley. A quantitative description of membrane current and its application to conduction and excitation in nerve. *J. Physiol.*, 117:500–544, 1952.

[13] F. C. Hoppensteadt and E. M. Izikevich. *Weakly Connected Neural Networks*. Springer-Verlag, New York, 1997.

[14] F. C. Hoppensteadt and C. Peskin. *Modeling and simulation in medicine and the life sciences. Second Edition*. Springer-Verlag, New York, 2001.

[15] T.B. Kepler, E. Marder, and L.F. Abbott. The effect of electrical coupling on the frequency of model neuronal oscillators. *Science*, 248:83–85, 1990.

[16] C. Koch and I. Segev. The role of single neurons in information processing. *Nature*, 3:1171–1177, 2000.

[17] Y. Kuramoto. *Chemical Oscillations, Waves, and Turbulence*. Springer-Verlag, Berlin, 1984.

[18] P. Lánský and R. Rodriguez. The spatial properties of a model neuron increases its coding range. *Biol. Cybern.*, 81:161–167, 1999.

[19] T.J. Lewis and J. Rinzel. Dynamics of spiking neurons connected by both inhibitory and electrical coupling. *J. Comp. Neurosci.*, 14:283–309, 2003.

[20] T.J. Lewis and J. Rinzel. Dendritic effects in networks of electrically coupled fast-spiking interneurons. *Neurocomputing*, 58-60:145–150, 2004.

[21] Z.F. Mainen and T.J. Sejnowski. Influence of dendritic structure on firing pattern in model neocortical neurons. *Nature*, 382:363–366, 1996.

[22] J.G. Mancilla, T.J. Lewis, D.J. Pinto, J. Rinzel, and B.W. Connors. Synchronization of electrically coupled pairs of inhibitory interneurons in neocortex. *J. Neurosci.*, 27(8):2058–2073, 2007.

[23] C. Morris and H. Lecar. Voltage oscillations in the barnacle giant muscle fiber. *Biophys J*, 35:193–213, 1981.

[24] J.C. Neu. Coupled chemical oscillators. *SIAM J. Appl. Math.*, 37(2):307–315, 1979.

[25] B. Pfeuty, G. Mato, D. Golomb, and D. Hansel. Electrical synapses and synchrony: The role of intrinsic currents. *J. Neurosci.*, 23(15):6280–6294, 2003.

[26] W. Rall. Membrane time constants of motoneurons. *Science*, 126:454, 1957.

[27] W. Rall. Membrane potential transients and membrane time constant of motoneurons. *Expt. Neurology*, 2:503–532, 1960.

[28] W. Rall. *Time constants and electrotonic length of membrane cylinders and neurons. In: Handbook of Physiology. The Nervous System I, Ed: J.M. Brookhart and V.B. Mountcastle.* American Physiological Society, Bethesda, MD, 1977.

[29] J. Rinzel and G.B. Ermentrout. *Analysis of neural excitability and oscillations. In: Koch C, Segev I (eds) Methods in neuronal modelling: from synapses to networks.* MIT Press, Cambridge, Mass. pp 135-171, 1989.

[30] A. A. Sharp, L. F. Abbott, and E. Marder. Artificial electrical synapses in oscillatory networks. *J. Neurophysiol.*, 67(6):1691–1694, 1992.

[31] F.K. Skinner, G.G. Turrigiano, and E. Marder. Frequency and burst duration in oscillating neurons and two-cell networks. *Biol. Cybern.*, 69:375–383, 1993.

[32] R.D. Traub and R. Miles. Pyramidal cell-to-inhibitory cell spike transduction explicable by active dendritic conductances in inhibitory cell. *J. Comp. Neurosci.*, 2(4):291–298, 1995.